Coster-Kronig factor f_{13} of $_{39}$Y measured with the synchrotron photoionization method

W. Jitschin, G. Grosse, and P. Röhl

Physikalisch-Technische Bundesanstalt, Institut Berlin, Abbestrasse 2-12, D-1000 Berlin 10, Federal Republic of Germany

The intensity of the L_3-$M_{4,5}M_{4,5}$ Auger line of $_{39}$Y excited by photons with energies in the range of the L_1 edge has been measured. It exhibits a jump at the edge due to the onset of the Coster-Kronig vacancy transfer from the L_1 to the L_3 subshell. From the measured jump ratio 1.13 ± 0.02 the Coster-Kronig yield $f_{13}=0.49\pm0.09$ is derived. This value agrees with a currently recommended value; however, it is significantly smaller than the prediction of recent relativistic calculations.

I. INTRODUCTION

Reliable information on the decay of inner-shell vacancies is of crucial importance in various fields ranging from fundamental atomic theory[1] via decisive studies of collision processes[2] to quantitative surface analysis.[3] Experimental data on decay yields are rather scarce and frequently suffer from large uncertainties.[4,5] In the case of heavy elements ($Z > 70$) significant progress in measuring these yields has recently been achieved in accuracy by the $K\alpha$-$L\alpha$ coincidence method[6-9] and in universality by the synchrotron photoionization method.[10-12] In contrast, in the case of light elements, experimental values of decay yields are practically nonexisting. Therefore we decided to apply the synchrotron photoionization method to light elements. The present paper reports on the promising result of a first test experiment.

II. EXPERIMENTAL PROCEDURE

In the synchrotron photoionization method, primary vacancies in the interesting subshells are created by photoionization and the vacancy decay is monitored. The ionization of a particular subshell is switched on or off by scanning the energy of the photons across its ionization edge. Thereby the Coster-Kronig vacancy transfer to higher-lying subshells is switched on or off. Concomitantly, the apparent (including the cascades) cross section of higher-lying subshell whose vacancy decay is monitored also exhibits a jump due to the onset of the cascades. The size of the jump allows us to derive the Coster-Kronig yield for the transition from the deeper-lying to the higher-lying subshell. In the case of the L vacancy decay of heavy elements ($Z > 70$) the induced x rays were used to monitor the vacancy decay.[10-12] This technique is less favorable in the case of light elements for various reasons: first, the x-ray yield is very small (typically less than 1%) and second, for low-energy x rays no detector with reasonable efficiency and sufficient energy resolution to resolve x rays originating from different L subshells is available. Therefore, we decided to monitor the vacancy decay by the emission of Auger electrons.

The experimental setup is sketched in Fig. 1. The synchrotron radiation from the Berliner Elektronen-Speicherring für Synchrotronstrahlung (BESSY) is monochromatized by the Kristall monochromator (KMC). The photon energy range from 2 to 2.5 keV is covered by using InSb (111) crystals which yield a larger photon flux than beryl, quartz, or Si crystals. Harmonics provide no problem since they occur at several times the characteristic energy (0.63 keV for BESSY), i.e., at energies where the intensity of the synchrotron radiation becomes insignificant. The energy scale of the monochromator is calibrated from a record of the total electron yield of the Y sample (Fig. 2) adopting the pronounced L edges whose energies are well known[13] as reference energies.

The monochromatized radiation is focused onto the sample by a toroidal mirror. A high-transparency (about 90%) Cu grid is mounted in the beam path; the grid current which originates from the induced photoemission is used to normalize the electron yield from the Y sample to the primary photon flux. Cu was chosen since it exhibits no absorption edges in the interesting energy range of the experiment (2–2.5 keV). In the sample chamber, ultrahigh-vacuum conditions prevail. The sample consists of a high-purity Y foil. Its surface was cleaned *in situ* at the start of the experiment by Ar$^+$ ion sputtering. Some minor O contamination could not be removed as can be seen from the 1s photoelectron line in the photoemission spectrum (Fig. 3). The surface of the sample did not change during the measurements as was checked by comparing photoemission spectra taken at the start and the end. The total photoyield of the sample is measured
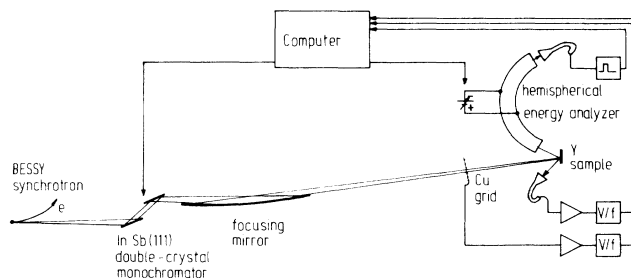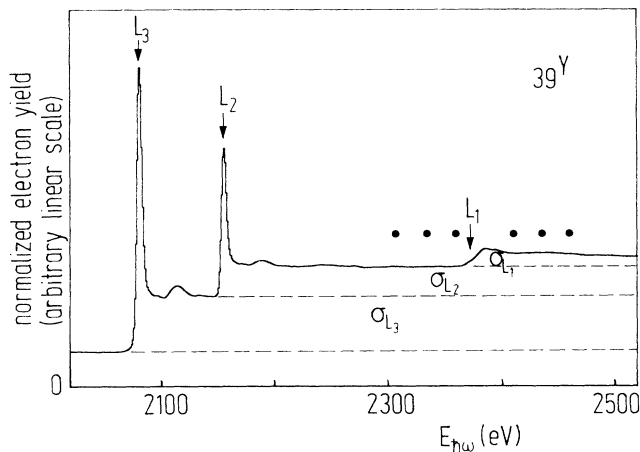

FIG. 1. Sketch of the experimental setup.

FIG. 2. Total electron yield of the Y sample normalized to the electron yield of the Cu grid vs primary photon energy. The dashed lines indicate the partitioning into the contributions from the individual L subshells. Energies at which the L_3-$M_{4,5}M_{4,5}$ Auger line was recorded are denoted by dots.
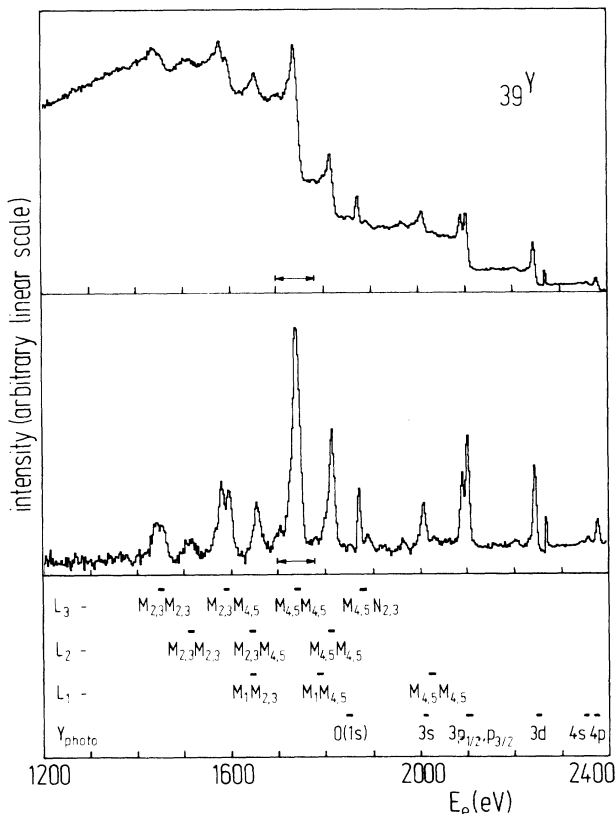

FIG. 3. Photoemission survey spectrum of the Y sample taken at photon energy of 2400 eV. Top, as measured; middle, after subtraction of a Shirley-type background [Eq. (4)]. The range over which the scans shown in Figs. 4 and 6 were taken is indicated. Bottom, identification of the lines according to tabulations (Refs. 13, 20, and 21).

with a channeltron multiplier. The electron spectra are recorded by a commercial hemispherical electron analyzer with 100-mm mean-sphere radius (CLAM 100 of Vacuum Generators); it is operated with 400-eV pass energy for recording survey spectra and with 200-eV pass energy for recording single lines. The energy resolution amounts to about 2% of the pass energy. The whole data acquisition is computer controlled.

A rough estimate of the intensities gives the following figures: monochromatized photon flux on sample 10^9/s (derived from measured photocurrent), yield of Auger electrons per incoming photon 10^{-3}, and acceptance of electron energy analyzer 10^{-3}. Thus one calculates a signal count rate in the strongest line of 10^3/s, in good agreement with the experimental value.

III. PHOTOIONIZATION CROSS SECTIONS

The data evaluation in the synchrotron photoionization method relies on accurate ratios of subshell cross sections. These can be taken from theoretical predictions as well as from experimental investigations. Relativistic Hartree-Slater (RHS) calculations[14] are expected to reproduce the experimental x-ray attenuation cross section of elements with $Z \approx 39$ at photon energies of a few keV with an absolute uncertainty of only a few percent.[15] The RHS calculations predict the following ratios for Y immediately above the L_1 edge[14]

$$\sigma_{L_1}/\sigma_{L_3} = 0.264, \quad \sigma_{L_2}/\sigma_{L_3} = 0.525 . \tag{1}$$

The energy dependence of these ratios is comparatively weak and can be neglected in the present case regarding the small investigated energy range. Alternatively, the subshell ionization cross sections can be determined by extrapolating photoabsorption cross sections beyond the absorption edges. Using synthesized (experimental and theoretical) cross-section data[16] we derive the following ratios:

$$\sigma_{L_1}/\sigma_{L_3} = 0.25, \quad \sigma_{L_2}/\sigma_{L_3} = 0.54 . \tag{2}$$

So far, we have assumed a smooth dependence of the cross sections on the photon energy by a power law. Actually, resonances near the threshold and extended x-ray absorption fine structure (EXAFS)[17] well above the threshold occur. In order to investigate their strength we have examined the total electron yield of the Y sample. Figure 2 shows the obtained data normalized to the electron yield of the Cu grid. The strong dependencies of the Y and Cu electron yields on photon energy apparently almost compensate each other so that the normalized signal hardly exhibits any energy dependence, except for edges. As can be seen from the figure, resonances at the L_3 and L_2 edges are strong, but a resulting disturbance of the Coster-Kronig measurements can be avoided by omitting the corresponding primary photon energies. The EXAFS fortunately is reasonably small.

The electron yield is approximately proportional to the photoionization cross section.[18] With the assumption that the yield is the same for all three individual L subshells, the relative jumps of the total electron yield at the

absorption edges directly give the relative ionization cross sections. From our data (Fig. 2) we get at those photon energies at which Auger emission spectra were recorded:

$$\sigma_{L_1}/\sigma_{L_3}=0.25-0.27, \quad \sigma_{L_2}/\sigma_{L_3}=0.54 \ . \tag{3}$$

The different data sets of the cross section ratios [Eqs. (1)–(3)] agree remarkably well, which may be fortuitous. One should keep in mind that the assumption of subshell-independent electron yields is questionable and that the measured normalized yield shows a remarkable decrease with increasing photon energy above the L_1 edge (Fig. 2) which is not expected. Therefore, we decided to adopt for the cross-section ratios the values given in Eq. (1) and assign an estimated uncertainty of $\pm10\%$ to them.

IV. PHOTOEMISSION SPECTRA

The recorded photoemission spectrum of Y normalized to the electron yield of the Cu grid is shown in Fig. 3, top; the primary photon energy was 2400 eV. This survey spectrum shows the characteristic lines as well as the low-energy tailing of each line. The tailing originates from electrons created at some depth in the sample which have experienced noticeable energy loss on their travel to the surface. Thus the measured signal S consists of a peak signal P originating from a surface layer of the sample (whose thickness is characterized by the mean-free path of the electrons) and a background contribution B originating from the bulk of the sample. In order to separate these two portions it has been suggested[19] that a peak signal P exhibits a low-energy background of energy-independent height αP. Under this assumption the measured signal can be decomposed into

$$S(i)=P(i)+B(i)$$

$$=P(i)+\alpha \sum_{j=i+1}^{i_{max}} P(j) \ , \tag{4}$$

where i denotes the channel number of the energy scale. Eq. (4) allows us to calculate the peak signal $P(i)$ from the measured $S(i)$ by an iterative procedure starting at the highest channel $i=i_{max}$ and progressing towards lower channels. Making a proper choice of α, the true peak signal P has been computed (Fig. 3, middle). This background-corrected spectrum shows the characteristic lines more clearly. The various lines can be easily identified using the known energies of the Auger electrons[20,21] and the binding energies for the photoelectrons.[13] No Auger lines originating from the L_1 subshell can be uniquely identified, presumably because they are too weak: The L_1 ionization cross section amounts to only 0.264 times the L_3 cross section [Eq. (1)], and the L_1 Auger yield amounts to only 0.21 times the L_3 Auger yield.[5] Accordingly the total L_1 Auger intensity amounts to only 0.05 times the L_3 total Auger intensity. The recorded Auger lines are broad, and some of them apparently split into several components. The broadening is due to the width of the involved levels caused by the

finite lifetime[22] and the solid-state band structure, whereas the splitting is due to a multiplet formation of the final two inner-shell vacancy state which has been analyzed in detail for the neighboring element $_{36}$Kr.[23]

For the determination of the Coster-Kronig yield f_{13} we consider the intensity of the L_3-$M_{4,5}M_{4,5}$ Auger line originating from the L_3 subshell which is the strongest line in the spectrum. This line was recorded with improved instrumental resolution (about 4 eV, according to the manufacturer's specifications, in agreement with the measured widths of photolines) at various energies of the primary photons in the regime of the L_1 edge, as indicated in Fig. 2. In order to determine the area of the Auger line, first a constant (i.e., independent of electron energy) background was fitted at the high-energy side of the line and subtracted. Then a subtraction of the low-energy tailing according to Eq. (4) was performed; the factor α was chosen (independent of the energy of the exciting photons) to bring the low-energy side of the peak approximately to zero. The result of this data evaluation is shown in Fig. 4. As can be seen, the L_3-$M_{4,5}M_{4,5}$ line consists of at least three components: The main peak corresponding to the $^1G_4$ configuration of the final state, the peak on the right shoulder of the line to the $^3F_{2,3,4}$ final configuration, and the peak at the left shoulder to the $^1S_0$ final configuration.[23] The spectra taken at photon energies above and below the L_1 edge clearly exhibit
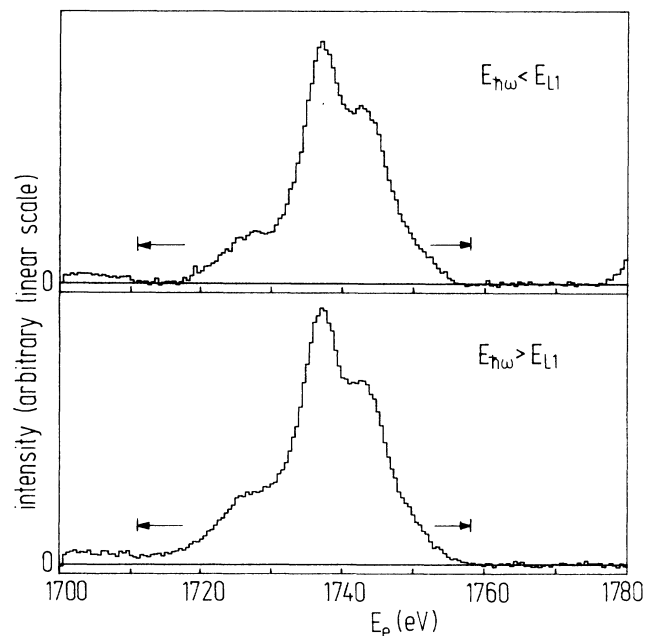

FIG. 4. Scan of the L_3-$M_{4,5}M_{4,5}$ Auger line of Y. The intensity is normalized to the electron yield of the Cu grid. A constant background and a Shirley-type background [Eq. (4)] have been subtracted, but no data smoothing has been performed. The energy of the exciting photons is below (spectrum B, top) or above (spectrum A, bottom) the L_1 edge. The integration interval for calculating the line area is indicated.

different shapes at the low-energy side. Since we are not interested in the detailed shape, no attempt was made to fit the line structure. In order to determine the line area, we simply take the integral over the peak; integration limits are indicated in Fig. 4.

V. DETERMINATION OF THE COSTER-KRONIG FACTOR f_{13}

The intensity of the L_3-$M_{4,5}M_{4,5}$ Auger line is proportional to the apparent L_3 ionization cross sections σ'_{L_3}, i.e.,

$$\sigma_{L_3'} = \sigma_{L_3} + f_{23}\sigma_{L_2} + (f_{13} + f_{12}f_{23})\sigma_{L_1} , \quad (5)$$

where the first term denotes direct L_3 ionization, whereas the second and third terms describe the vacancy transfer by cascades from the L_2 and L_1 subshells, respectively, to the L_3 subshell. The jump ratio R of the L_3-$M_{4,5}M_{4,5}$ intensity at the L_1 edge, i.e., the ratio of the line intensity at photon energies immediately below the L_1 edge to the intensity at photon energies immediately above the L_1 edge, is given by

$$R = \frac{\sigma_{L_3} + f_{23}\sigma_{L_2} + (f_{13} + f_{12}f_{23})\sigma_{L_1}}{\sigma_{L_3} + f_{23}\sigma_{L_2}} . \quad (6)$$

This equation can be rewritten to give f_{13} as a function of R:

$$f_{13} = (R-1)(\sigma_{L_3}/\sigma_{L_1} + f_{23}\sigma_{L_2}/\sigma_{L_1}) - f_{12}f_{23} . \quad (7)$$

For the uncertainty Δf_{13} of f_{13} we get

$$(\Delta f_{13})^2 = [(\sigma_{L_3}/\sigma_{L_1} + f_{23}\sigma_{L_2}/\sigma_{L_1})\Delta R]^2$$

$$+ [(R-1)\Delta(\sigma_{L_3}/\sigma_{L_1})]^2$$

$$+ [(R-1)f_{23}\Delta(\sigma_{L_2}/\sigma_{L_1})]^2 . \quad (8)$$

The cross-section ratios have already been determined (see Sec. III), and the values of Eq. (1) are adopted with uncertainties of 10%. The Coster-Kronig factors f_{12} and f_{23} are small and play only the role of corrections. It is thus justified to adopt recommended values $f_{12}=0.26$, $f_{23}=0.126$ and to neglect their uncertainties.[5] Inserting the numerical values one obtains

$$f_{13} = (R-1)(3.788 + 0.126 \times 1.989) - 0.26 \times 0.126$$

$$= (R-1)4.038 - 0.033 \quad (9)$$

and

$$(\Delta f_{13})^2 = (4.038\Delta R)^2 + [0.38(R-1)]^2 . \quad (10)$$

The uncertainty Δf_{13} of f_{13} has two contributions originating from the uncertainty of the emission jump ratio R and the uncertainty of the ratios of ionization cross sections. Equation (7) allows us to determine f_{13} from the measured intensity jump R of an Auger line originating from the L_3 subshell. The jump ratio R is obtained from our experimental data by two independent methods of data evaluation.

In the first method, the measured dependence of the normalized L_3-$M_{4,5}M_{4,5}$ Auger intensity $I(E)$ on photon energy E is used. The Auger signal is proportional to the apparent L_3 cross section of Y; the photoyield of the Cu grid used for normalization is proportional to $\mu(E)Ef(E)$, where $\mu(E)$ is the x-ray attenuation coefficient and $f(E)$ a slowly varying function of E.[18] Thus the normalized Auger intensity is expected to behave as

$$I(E) \propto \frac{\sigma_{L_3'}(E)}{\mu(E)Ef(E)} . \quad (11)$$

Except for the absorption edges, the energy dependence of $I(E)$ should be approximately E^{-1}, since the dependencies of $\sigma_{L_3'}(E)$ and $\mu(E)$ are rather equal and almost cancel.[24] However, out data show a different behavior (Fig. 5). Therefore it was decided to fit the data by the ansatz

$$I(E) \propto E^n \begin{cases} 1 & \text{below the } L_1 \text{ edge} \\ R & \text{above the } L_1 \text{ edge} \end{cases} \quad (12)$$

with free parameters n, R. The best fit was obtained with $n = 0.7$ and $R = 1.115 \pm 0.030$. The uncertainty stems mainly from the considerable drift between the individual runs (about 10%) which were performed within a few days, as can be seen from the shift of the data from individual runs (Fig. 5). Possible reasons of the drift are changes of the position of the primary photon beam or of the gain of the electron multiplier at the energy analyzer.

This drift problem is avoided in the second method to determine R. The basic idea in this method is that the L_3-$M_{4,5}M_{4,5}$ Auger line changes not only its intensity but also its shape when the primary photon energy is scanned over the L_1 edge: The L_1-L_3 Coster-Kronig vacancy decay creates an $M_{4,5}$ vacancy in about 90% of all
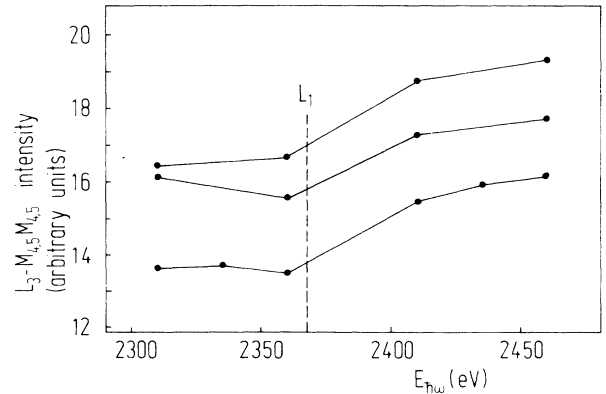

FIG. 5. Intensity of the L_3-$M_{4,5}M_{4,5}$ Auger line normalized to the electron yield of the Cu grid at various primary photon energies. Dotted points are the experimental data; the straight lines connect the data of single measuring runs. An instrumental drift of the intensity between and during the individual runs is clearly visible.

cases,[25] which, as a spectator, causes a shift of the L_3-$M_{4,5}M_{4,5}$ Auger line of Y by about -10 eV.[26] Such a shift is larger than the linewidth and is experimentally resolved.

Indeed, Auger spectra taken at photon energies below (designated by B) and above (designated by A) the L_1 edge exhibit significantly different shapes (Fig. 4). If one assumes that the high-energy side of the Auger line originates solely from direct L_3 ionization, a matching of the spectra A,B at the high-energy side according to the condition $sA=B$ with proper chosen scaling factor s then relates both spectra to the same strength of the direct L_3 ionization. Then the jump ratio R_M (M denotes the existence of an M spectator vacancy) is just

$$R_M = \int sA \Big/ \int B ,\tag{13}$$

where the integration denotes the line area. To get good statistics for a quantitative analysis, we summed all Auger spectra taken either below or above the L_1 edge (Fig. 4). The matching of the spectra was judged from the difference sA-B (Fig. 6). The difference spectrum which represents the L_3-$M_{4,5}M_{4,5}$ satellite for an M spectator vacancy has a different shape and is broader than the diagram line. This feature is attributed to the different multiplet splittings of the final states for both lines, i.e., a three-vacancy state for the satellite line and a two-vacancy state for the diagram line. For the case of best matching, a jump ratio $R_M = 1.13\pm0.02$ was obtained. The value for R is somewhat larger than R_M,
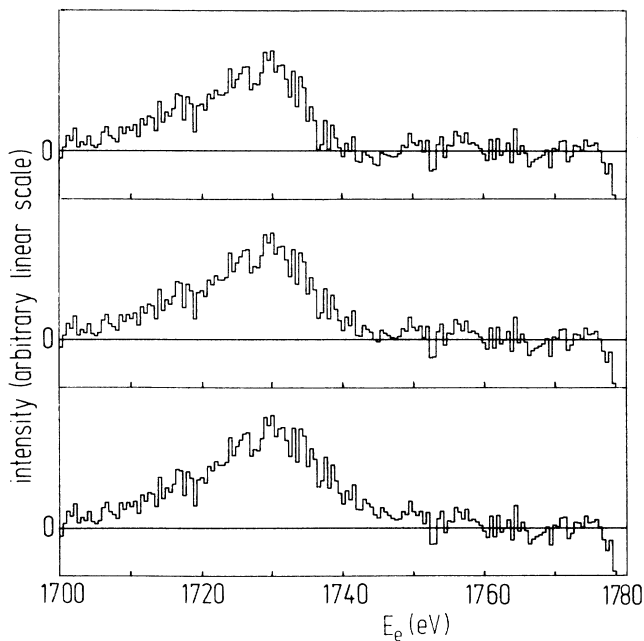

FIG. 6. Difference of the L_3-$M_{4,5}M_{4,5}$ Auger spectra A taken at photon energies above the L_1 edge (Fig. 4, bottom) and B taken at photon energies below the L_1 edge (Fig. 4, top). Top, 0.95 A-B; middle, 0.97 A-B; bottom, 0.99 A-B. The vertical scale is four times enlarged compared to the vertical scale in Fig. 4.

adopting theoretical branching ratios of the L_1-L_3 Coster-Kronig decay[25] one gets $R-1=(R_M-1)/0.89$ and thus $R=1.146\pm0.022$.

Combining the results for the jump ratio R obtained by the two methods of data evaluation we arrive at the final value

$$R=1.13\pm0.02 .\tag{14}$$

Inserting this value of R into Eqs. (9) and (10) the final result for the Coster-Kronig yield f_{13} of $_{39}$Y is obtained:

$$f_{13}=0.49\pm0.09 .\tag{15}$$

The main contribution to the uncertainty of f_{13} stems from the uncertainty of determining the jump ratio R, whereas the uncertainties of the cross-section ratios give a smaller contribution.

VI. DISCUSSION OF THE RESULT

Our value of f_{13} [Eq. (15)] is in nice agreement with the value adopted in a widespread tabulation $f_{13}=0.52\pm0.05$.[5] The only other experimental value known to the authors has been obtained from an analysis of the satellite structure of the x-ray fluorescence and is the partial yield $f_{13M}=0.40$.[27] The index M denotes that fraction of all L_1-L_3 Coster-Kronig transitions in which a final L_3M vacancy state is created. Adopting the relative strengths of the various Coster-Kronig transitions from theory[25] we get $f_{13M}=0.89f_{13}$. With this relation the reported f_{13M} value can be converted to give $f_{13}=0.45$, which also agrees nicely with our result.

It is a challenging task to compare our experimental f_{13} value to theory. Calculated absolute decay rates are available for the neighboring element $_{40}$Zr, and we tacitly assume that the decay rates of $_{40}$Zr and of the experimentally measured $_{39}$Y are approximately the same. Our experimental value $f_{13}=0.49$ is smaller than various theoretical predictions $f_{13}=0.648,$[28] $f_{13}=0.522,$[29] and $f_{13}=0.747.$[1] We now try to trace the origin of the discrepancy. The radiative decay can be excluded due to its small contribution to the total L_1 decay, which amounts to less than 1% according both to theory[28,29,1] and experiment.[30] The strongly prevailing decay of L_1 vacancies occurs by nonradiative processes. The Coster-Kronig factor f_{13} probes the relative strengths of the various nonradiative L_1 decay transitions. Theoretical intensities[25] and energies[31] of these transitions are displayed in Fig. 7. The L_1-$L_3M_{4,5}$ line has overwhelming strength, giving a contribution of about 4 eV to the L_1 level width. On the other hand, a recent experimental investigation gives a total L_1 level width of $_{40}$Zr of 3.5 eV (Ref. 27), in fair agreement with a semiempirical value of 4.8 eV.[22] From the total L_1 level width we can conclude that theory apparently significantly overestimates the strength of this line. From the experimental numbers 3.5 eV of the L_1 level width[27] and 0.49 of the f_{13} yield (present work) we calculate a L_1-L_3 Coster-Kronig partial width $\Gamma(f_{13})=1.7$ eV; this value is smaller than theoretical predictions (Fig. 8) by a factor of about 2.5.
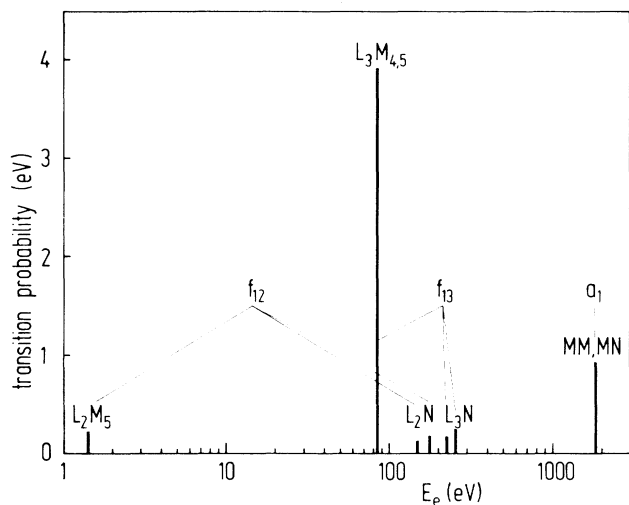
FIG. 7. Theoretical prediction for the nonradiative decay of the L_1 subshell of $_{40}$Zr (Refs. 25 and 31). The final two-vacancy state is indicated.

FIG. 8. Partial level widths of $_{40}$Zr for the Auger and Coster-Kronig decay of L_1 vacancies as predicted by theory. Nonrelativistic calculations: (a) from Ref. 28, (b) from Ref. 29. Relativistic calculation: (c) from Ref. 1.

For the summed partial widths of the L_1-L_2 Coster-Kronig and the Auger decay we obtain experimentally $\Gamma(f_{12})+\Gamma(a_1)=\Gamma(L_1)-\Gamma(f_{13})=1.8$ eV; this value is larger than the nonrelativistic predictions by a factor of about 1.8 but roughly agrees with the relativistic prediction (Fig. 8). These results confirm and refine the earlier general statement that theoretical Coster-Kronig rates for the L_1 subshell of Zr "are too high by a factor of about 2."[32]

A striking difference between nonrelativistic and relativistic theories are the predictions of the f_{12} Coster-Kronig rate which differ by as much as a factor of 4 (Fig. 8). Experimental studies of f_{12} are therefore highly desirable. These can be performed by the same method as used in the present work on f_{13} but detecting the L_2-$M_{4,5}M_{4,5}$ Auger line instead of the L_3-$M_{4,5}M_{4,5}$ Auger line.

An overestimate of the f_{13} and f_{12} Coster-Kronig yields by theory has also been found for heavy elements $(Z \geq 72)$.[12] It had been attributed to inadequacy of the frozen-core, central-field approximation for calculating nonradiative transition probabilities of such transitions in which the outgoing electron is comparatively slow and has sufficient time to interact with the bound electrons in the remaining ions. The results of the present work thus corroborate the statement that for $Z < 49$ a need exists for a many-body calculation of low-energy L_1-$L_{2,3}M_{4,5}$ Coster-Kronig transitions.[1]

VII. CONCLUSION

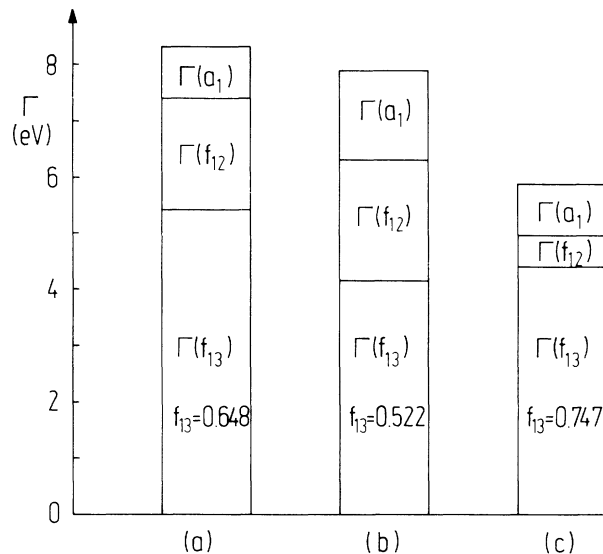The novel synchrotron photoionization method is well suited for measuring vacancy decay yields also for light elements. The present work has demonstrated the feasibility of such measurements in which the induced electron emission is detected. The achieved uncertainty is sufficient to draw decisive conclusions on theoretical predictions. A significant reduction of the uncertainties by minor experimental improvements seems feasible: The background under the Auger lines can be strongly reduced by using a thin film of the sample material evaporated on a material with low x-ray absorption and low-electron backscattering. A very accurate method of normalization can be realized by employing a two-element sample and recording lines from the second element simultaneously. It remains a challenging task to perform corresponding measurements on a series of light elements since drastic changes of Coster-Kronig yields are expected at some atomic numbers Z at which individual decay channels become energetically forbidden or allowed.

[1]M. H. Chen, B. Crasemann, and H. Mark, Phys. Rev. **24**, 177 (1981).

[2]W. Jitschin, A. Kaschuba, R. Hippler, and H. O. Lutz, J. Phys. B **15**, 763 (1982).

[3]W. Jitschin and U. Werner, J. Vac. Sci. Technol. A **5**, 1203 (1987).

[4]P. V. Rao, in *Atomic Inner-Shell Processes,* edited by B. Crasemann (Academic, New York, 1975), Vol. II, p. 1.

[5]M. O. Krause, J. Phys. Chem. Ref. Data **8**, 307 (1979).

[6]M. Tan, R. A. Braga, R. W. Fink, and P. V. Rao, Phys. Scr. **25**, 536 (1982).

[7]J. L. Campbell, P. L. McGhee, R. R. Gingerich, R. W. Ollerhead, and J. A. Maxwell, Phys. Rev. A **30**, 161 (1984).

[8]A. L. Catz, Phys. Rev. A **36**, 3155 (1987).

[9]J. L. Campbell and P. L. McGhee, J. Phys. (Paris) Colloq. **48**, C9-597 (1987); P. L. McGhee and J. L. Campbell, J. Phys. B **21**, 2295 (1988).

[10]W. Jitschin, G. Materlik, U. Werner, and P. Funke, J. Phys. B **18**, 1139 (1985).

[11]U. Werner and W. Jitschin, J. Phys. (Paris) Colloq. **48**, C9-559 (1987).

[12]U. Werner and W. Jitschin, Phys. Rev. A **38**, 4009 (1988).

[13]J. A. Bearden and A. F. Burr, Rev. Mod. Phys. **39**, 125 (1967).

[14]J. H. Scofield, Lawrence Livermore Radiation Laboratory Report No. UCRL-51326, 1973 (unpublished).

[15]E. B. Saloman, J. H. Hubbell, and J. H. Scofield, At. Data Nucl. Data Tables **38**, 1 (1988).

[16]B. L. Henke, P. Lee, T. J. Tanaka, R. L. Shimabukuro, and B. K. Fujikawa, At. Data Nucl. Data Tables **27**, 1 (1982).

[17]P. A. Lee, P. H. Citrin, P. Eisenberger, and B. M. Kincaid, Rev. Mod. Phys. **53**, 769 (1981).

[18]B. L. Henke, J. A. Smith, and D. T. Atwood, J. Appl. Phys. **48**, 1852 (1977).

[19]D. A. Shirley, Phys. Rev. B **5**, 4709 (1972).

[20]W. A. Coghlan and R. E. Clausing, At. Data **5**, 317 (1973).

[21]F. P. Larkins, At. Data Nucl. Tables **20**, 311 (1977); **23**, 587 (1979).

[22]M. O. Krause and J. H. Oliver, J. Phys. Chem. Ref. Data **8**, 329 (1979).

[23]J. C. Levin, S. L. Sorensen, B. Crasemann, M. H. Chen, and G. S. Brown, Phys. Rev. A **33**, 968 (1986).

[24]K. F. J. Heinrich, in *The Electron Microprobe,* edited by T. D. McKinley, K. F. J. Heinrich, and D. B. Wittry (Wiley, New York, 1966), p. 296.

[25]M. H. Chen, B. Crasemann, and H. Mark, At. Data Nucl. Data Tables **24**, 13 (1979).

[26]S. B. Whitfield, G. B. Armen, R. Carr, J. C. Levin, and B. Crasemann, Phys. Rev. A **37**, 419 (1988).

[27]J. Q. Xu and E. Rosato, J. Phys. (Paris) Colloq. **48**, C9-661 (1987).

[28]E. J. McGuire, Phys. Rev. A **3**, 587 (1971).

[29]B. Crasemann, M. H. Chen, and V. O. Kostroun, Phys. Rev. A **4**, 2161 (1971).

[30]J. Auerhammer, H. Genz, and A. Richter, Z. Phys. D **7**, 301 (1988).

[31]M. H. Chen, B. Crasemann, K.-N. Huang, M. Aoyagi, and H. Mark, At. Data Nucl. Data Tables **19**, 97 (1977).

[32]M. O. Krause, F. Wuilleumier, and C. W. Nestor, Jr., Phys. Rev. A **6**, 871 (1972).